Available online at www.sciencedirect.com
ScienceDirect
Advances in Space Research 47 (2011) 1823–1832
ADVANCES IN SPACE RESEARCH (a COSPAR publication)
www.elsevier.com/locate/asr

Forest biomass monitoring with GNSS-R: Theoretical simulations

P. Ferrazzoli [a], L. Guerriero [a,*], N. Pierdicca [b], R. Rahmoune [a]

[a] Dipartimento di Informatica, Sistemi e Produzione, Università di Roma "Tor Vergata", Via del Politecnico 1, 00133 Rome, Italy
[b] Dipartimento di Ingegneria Elettronica, Università di Roma "La Sapienza", Via Eudossiana 18, 00184 Rome, Italy

Received 12 October 2009; received in revised form 6 April 2010; accepted 17 April 2010
Available online 28 April 2010

Abstract

GNSS-Reflectometry (GNSS-R) is a remote sensing technique which performs bistatic measurements of the earth surface scattering. This paper presents some theoretical simulations of the specular scattering coefficient of a forested area, with the aim of demonstrating the potentiality of GNSS-R in monitoring forest biomass. The study is performed by means of an electromagnetic model developed in the past years and tested over several vegetation covered sites in its active and passive version. Here, after showing a comparison between model results and measurements over a forest site in the monostatic configuration, and after summarizing other previous validations, the extension to the specular configuration, typical of GNSS-R systems, will be presented. Namely, simulations are carried out at circular polarization and a sensitivity analysis of the received power in the specular configuration to some soil and forest parameters is shown.

In the GNSS-R configuration, the theoretical response of vegetation shows a decreasing trend with increasing biomass, due to the increasing attenuation by the plant canopy which reduces the coherent scattering from the soil. The latter, however, remains higher than incoherent scattering even when forest biomass is large, especially at RL polarization and low incidence angle. Consequently the magnitude of the received power is sensitive to the forest biomass without exhibiting the typical saturation of radar backscattering measurements, and it may thus allow biomass retrieval.

Keywords: Electromagnetic models; Bistatic scattering; Vegetation; Soil moisture

1. Introduction

GNSS-Reflectometry is gaining increasing interest in the remote sensing community, due to the bistatic nature of the microwave scattering measurements (Jin and Komjathy, 2010). This technique exploits the L-band Global Navigation Satellite System (GNSS) signal as an opportunity source, with the consequent advantages of a limited cost and a potential high time resolution when performed from a spaceborne platform (Ruffini, 2006). Most of GNSS-R activities, both theoretical and experimental (Zavorotny and Voronovich, 2000a; Hajj and Zuffada, 2003; Martin-Neira et al., 2001; Gleason et al., 2005) concern oceans, as the high conductivity maximizes the reflected signal amplitude. Although most works considered the altimetric application, aimed at estimating the delay between direct and reflected signals, also the scatterometric mode is gaining interest. The latter measures the power coming from the sea surface, with the objective of estimating the reflection properties of the observed area which, on their side, are related to the sea state and wind speed over the ocean.

Recently, the scatterometric mode has been proposed for land applications also, i.e., soil moisture monitoring (Masters et al., 2004) since, according to the well established Fresnel formulas, the reflection coefficient of a flat surface depends on its permittivity which, in the case of land, is dependent on its moisture content. Semi-empirical permittivity models indicate L-band to be well sensitive to this parameter, so that an appreciable sensitivity of GNSS-R to soil moisture is expected. In the last decade some experimental campaigns were carried out to demonstrate that GNSS-R power waveforms can be detected over land, and their parameters are correlated to soil moisture content

* Corresponding author.
E-mail address: guerriero@disp.uniroma2.it (L. Guerriero).

0273-1177/$36.00 © 2010 COSPAR. Published by Elsevier Ltd. All rights reserved.
doi:10.1016/j.asr.2010.04.025

(Zavorotny et al., 2003; Masters et al., 2004; Gleason, 2006). Most of the pioneering study were devoted to a qualitative interpretation of the land waveforms, while most recent works proposed inversion algorithms relating power value of the waveforms to the Fresnel reflectivity (Katzberg et al., 2006; Egido et al., 2008). The sensitivity to soil moisture of the GPS reflected signal was proved also by means of a different approach: the Interferometric Pattern Technique (Rodriguez-Alvarez et al., 2009), which is based on the coherent addition of the direct and reflected fields.

A theoretical study was performed by Zavorotny and Voronovich (2000b) who extended a previous model, based on the Geometrical Optics approximation and concerning GPS scatterometry over ocean, to the case of a bare soil with rough surface. The work in Pierdicca et al. (2008) also analyses the sensitivity to soil moisture of bare soil bistatic scattering, showing that at L-band the specular configuration exhibits a high sensitivity.

The presence of vegetation can make the soil moisture retrieval a difficult task, since it attenuates and scatters the GNSS signal before it impinges on the ground and after it is reflected to the receiver (Katzberg et al., 2006). On the other hand, this may suggest another application of GNSS scatterometry, i.e. vegetation monitoring. It is well known that the biomass dependency of the radar backscatter varies as a function of radar wavelength and polarization, though reaching saturation after a certain biomass level. In Ferrazzoli et al. (2000) model simulations were carried out at L- and C-band with the aim of assessing the relevant features and the potential of the bistatic technique, and to investigate the possibility to overcome the limitations of monostatic radar in monitoring the crop biomass. Although the work was not strictly related to the use of GNSS-R, it considered specular scattering, so that its results at L-band may be taken as a first example of the potentiality of this technique. The theoretical study, carried out by means of a discrete Radiative Transfer model, showed that the biomass range over which an appreciable measurement dynamics is maintained can be widened by the specular bistatic configuration (Ferrazzoli et al., 2000). In particular, it was shown that the co-polar linear responses of a sunflower crop exhibits a decreasing trend with increasing biomass, since scattering in the specular direction is dominated by the soil coherent component, while all incoherent contributions are several dB's lower than total specular scattering.

In this paper, we extend the previous study on specular scattering focusing on GNSS-R applications to biomass monitoring of forests. The latter covers a very important role within the global monitoring objectives of remote sensing, such as carbon modelling, greenhouse gas emission inventories and deforestation control. Collection of GNSS signal reflections over land may represent a valuable tool to monitor the vegetation biomass, complementing the already well assessed capability of GNSS-R over the sea surface.

In Section 2 the discrete electromagnetic model which has been used to carry out this study will be recalled, and the equations adopted to estimate the variables required by the model will be shown. In Section 3, previous validations of the model will be summarized. Also, a specific forest site for which radar measurements were made available by literature will be considered (Imhoff, 1995) and a specific validation in the monostatic configuration will be carried out. The specular scattering coefficient of the same forest site will be then simulated at VV and HH polarizations. In order to take into account the polarization properties of the GPS signal, in Section 4 we will simulate the circular polarized scattering coefficient using a simplified version of the model. Finally, parametric simulations will be carried out using the typical GNSS parameters, in order to estimate the potentialities of GNSS-Reflectometry.

2. Model description

2.1. The electromagnetic model

The model developed at Tor Vergata University, which has been used in this study, is a discrete model, i.e., it represents the vegetated surface by means of a rough surface covered by an ensemble of lossy dielectric elements of simple shape. In the development of a discrete model, the first step consists in identifying the elements composing the vegetation structure, and assigning them realistic locations within the canopy. Then, simplified geometrical shapes are selected and associated to vegetation elements, in order to describe their scattering and absorption properties by means of analytical expressions developed on the basis of electromagnetic theories. Thus, in the case of forests, the considered elementary scatterers are cylinders, able to model trunks and branches, disks to model broad leaves, and needles, when conifer leaves are present. In the Tor Vergata model, the bistatic scattering properties of cylinders are simulated applying the Infinite Cylinder approximation (Karam and Fung, 1988), while the Generalized Rayleigh Gans (Eom and Fung, 1984, 1986) or the Physical Optics (Le Vine et al., 1983) approximations are applied for disks and needles, depending on the object size with respect to the wavelength. These are the canonical approximations currently applied in microwave active models (Liang et al., 2005).

The layer containing the ensemble of scatterers lies on a lossy dielectric homogeneous half space (representing the soil) with a rough interface. In the case of forests, soils are often covered by litter and/or understory vegetation that may modify soil properties. Following the procedure described in Della Vecchia et al. (2007), the whole soil–litter medium is reduced to a unique homogeneous half-space of given permittivity, which is usually lower than that of soil – except in the case of very dry soil. On its side, understory is represented as an absorbing layer.

A detailed description of the Tor Vergata model can be found in Ferrazzoli and Guerriero (1995), where it is shown how the scattering and extinction properties of each scatterer are combined using the Matrix Doubling algorithm. This method allows to take multiple scattering into account

and yields a scattering matrix of the whole soil-vegetation canopy, whose elements are functions of both the incidence and scattering directions. Thus, the Tor Vergata model is intrinsically bistatic: for this reason a passive version was directly generated by applying the energy conservation law. This passive model is able to simulate microwave radiometric measurements of vegetation (Ferrazzoli and Guerriero, 1996), while the first bistatic simulations are shown in Ferrazzoli et al. (2000) in the case of crops.

It is well known that, due to the low power flux density at the earth surface, the reflected GNSS signal is significantly high in the specular direction only, so that the simulations presented in this paper will refer to this direction. Specifically, the specular scattering coefficient of the forest canopy is modelled by

$$\sigma^0_{pq}(\vartheta_i, \vartheta_s = \vartheta_i, \varphi_s - \varphi_i = 0) = \sigma^{0coh}_{pq}(\vartheta_i, \vartheta_i, 0) + \sigma^{0inc}_{pq}(\vartheta_i, \vartheta_i, 0) \quad (1)$$

where ϑ_i and φ, ϑ_s and φ_s describe the zenith and azimuth direction of, respectively, the incident and scattered electromagnetic fields; p and q stand for polarizations of the scattered and incident electromagnetic fields. σ^{0coh}_{pq} is the coherent scattering coefficient of the soil attenuated by the above lying vegetation canopy. This coherent component is computed following the theory developed in Fung and Eom (1983) which correctly takes into consideration the spherical shape of the wave front impinging on the surface when produced by a real antenna. Note that the coherent scattering coefficient of the soil depends not only on the surface parameters, but also on the receiving and transmitting antenna parameters. σ^{0inc}_{pq} is the incoherent scattering coefficient of the whole soil-vegetation canopy: it includes volume scattering from leaves and branches, double bounce effects due to soil and trunk interactions, multiple interactions between vegetation elements and between vegetation and the soil, incoherent scattering from the soil attenuated by the overlying vegetation canopy. The latter contribution is simulated by means of the Integral Equation Method (Fung, 1994), which was developed to fill the gap in the applicability range of the Kirchoff and Small Perturbation approaches. Although it contains some approximations which have been improved by subsequent versions (advanced IEM, IEM with multiple scattering), the original bistatic version is considered accurate in many practical cases, especially at L-band and for typical roughness parameters of soil (Macelloni et al., 2000; Chen et al., 2003). Furthermore, in Section 3.3 it will be shown that scattering in the specular direction is strongly influenced by soil coherent scattering, so that eventual inaccuracies of the IEM predictions can be taken as negligible in this direction.

2.2. The forest parameters

The model requires as input the moisture and roughness parameters of the soil, the litter dry biomass, and the tree density. Moreover, for each of the three main forest components, i.e. trunks, branches and leaves, it is necessary to give the overall volumes, the permittivity, the distribution of dimensions and the distribution of orientations. The method adopted in this work uses various kinds of relationships among variables, as well as information available in the literature, in order to run the model with input variables which are restricted in number and reasonably available in real cases. In particular, the procedure assumes to know, besides soil variables, the following inputs:

- tree density N_T (ha^{-1}),
- total dry biomass per unit area $DB0$ (t/ha),
- distribution of trunk diameters at breast height dbh (cm) (the probability density function $p(dbh)$), with its mean value dbh_{mean}, its standard deviation σ_{dbh} and its range $dbh_{max} - dbh_{min}$,
- the Leaf Area Index LAI,
- moisture m (g/g) and dry matter density ρ_D (g/cm^3) of trunks, branches and leaves.

Using allometric equations and empirical formulas derived by literature (Jenkins, 2003; Cannell, 1982), the geometrical and physical variables required by the electromagnetic model can be computed, according to the procedure indicated in detail by Della Vecchia et al. (2010).

In the following Section 3.2, backscattering measurements at L-band over a forest site in Hawaii (Imhoff, 1995) are compared with model simulations and, afterwards, simulations of the specular scattering coefficient of the same forests will be carried out in Section 3.3. The Hawaii site is an evergreen broadleaf forest (*Metrosideros polimorpha*) with varieties appearing as small shrubs and tall trees (Imhoff, 1995). In that paper, dbh measurements in a range within 2 and 21 cm are reported for a biomass range between 4 and 300 t/ha: these values were used as a guideline to hypothesize a linear increase of dbh_{mean} (cm) with forest biomass $DB0$ (t/ha). Since no further details were given about the relationship between these variable, a simple linear correlation was supposed in agreement with measurements collected over other forest sites (Le Toan et al., 1992). Model simulations were performed using a dbh distribution of Gaussian type, with $dbh_{mean} = (0.036 * DB0) + 6.3$ and standard deviation $\sigma_{dbh} = dbh_{mean}/3$. The dbh range defined previously was calculated fixing $dbh_{min} = dbh_{mean} - 3\sigma_{dbh}$ (setting a lower limit $dbh_{min} = 2$ cm) and $dbh_{max} = dbh_{mean} + 3\sigma_{dbh}$. Also for LAI a linear increase with biomass was supposed, i.e., $LAI = DB0/50$. The tree density [#/ha] was calculated by means of

$$N_T = 10^3 \left(a \left(\frac{DB0}{b} \right)^{c-1} \exp\left(- \left(\frac{DB0}{b} \right)^{c} \right) \right)$$
$$a = 14.3 \quad (2)$$
$$b = 232.42$$
$$c = 1.49$$

which was derived performing a best fitting of the densities reported at the bottom of Fig. 1 in Imhoff (1995). Eq. (2) is reproduced in Fig. 1. All necessary forest parameters were then derived according to the procedure described in Della Vecchia et al. (2010).

3. Model simulations over a specific site

3.1. Previous comparisons of the model with experimental data

The Tor Vergata model for forests was originally developed to study the sensitivity of radar backscattering to biomass and tree geometrical properties. In Ferrazzoli and Guerriero (1995), the monostatic simulations of the Tor Vergata model were compared against backscattering coefficients of the Flevoland site (The Netherlands) collected during the MAESTRO-1 campaign in 1991. L-band data were acquired over five deciduous forests with different biomasses and were reproduced by the model with a slight overestimation.

Applying the energy conservation and reciprocity principles, it was demonstrated (Peake, 1959) that emissivity is related to the integral of the bistatic scattering coefficient carried over all scattering directions in the upper half space Ω_s:

$$e_p(\vartheta_i) = 1 - \frac{1}{4\pi \cos\vartheta_i} \int_{\Omega_s} (\sigma^0_{pp}(\vartheta_i, \vartheta_s, \varphi_s) + \sigma^0_{pq}(\vartheta_i, \vartheta_s, \varphi_s)) d\Omega_s \quad (3)$$

As it was mentioned in the previous section, the intrinsic bistatic nature of the Tor Vergata model allowed us to develop a passive version which is able to simulate the emissivity of a forest environment (Ferrazzoli and Guerriero, 1996) on the basis of the previous integral equation. The emissivity simulations were validated against multitemporal data collected during the ground based Bray experiments (Della Vecchia et al., 2007) carried out over a single site in Les Landes forests (France). This study has demonstrated the sensitivity of forest emission at L-band to Soil Moisture and the important effect of litter. More recently, the comparison of model outputs with airborne measurements carried out in Tuscany (Italy) over forests of different species showed that emissivity is reproduced with a significant accuracy (in the range 2–3 K) and it allowed to single out the effects of Soil Moisture, forest biomass and trunk diameter (Della Vecchia et al., 2010).

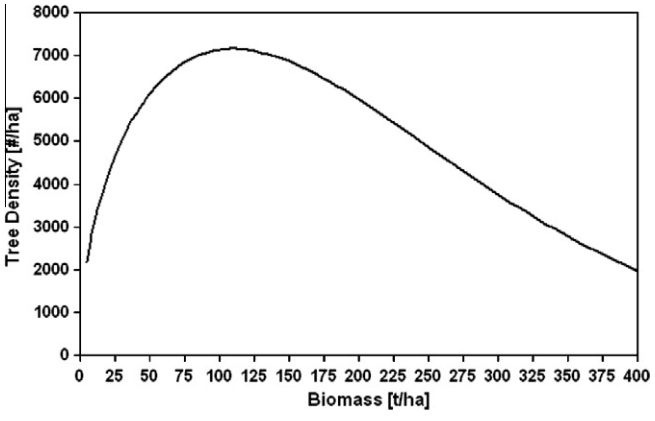

Fig. 1. Tree density of the Hawaii forest site used to perform backscattering and specular simulations.

Validation of the bistatic scattering simulations has not been possible, up to now, due to the lack of experimental data. However, the comparisons of both backscattering and emissivity with experimental data allow us to rely on the global performance of the bistatic model, since both scattering in a single direction, i.e., the backward direction, and the integral of scattering in the whole upper hemisphere, are reproduced with a satisfactory accuracy. In particular, we note that emissivity at L-band is strongly affected by coherent scattering in the specular direction which, as it will be shown in Section 3.3, is the scattering component mainly affecting the GNSS-R measurements.

3.2. Backscattering simulation test

In the past, several campaigns were carried out with the NASA/JPL AIRSAR in order to study the correlations between radar backscatter and forest parameters. They were accompanied by ground measurements like those performed at the Duke forest site in North Carolina (USA) (Kasischke et al, 1994), Les Landes in France (Le Toan et al., 1992) and Hawaii (Imhoff, 1995). In this paper, backscattering measurements at L-band over the latter site are compared with simulations performed with the Tor Vergata model; to this aim we use the polynomial regression curves reported in Imhoff (1995) to reproduce the experimental trend of the three linearly polarized backscattering coefficients as a function of the forest biomass. The SAR observation angle ranged between 40° and 50°, and in our simulations it has been fixed to 45°.

In the absence of information about the soil parameters, typical average values of soil moisture and roughness of vegetated soils were assumed: the Soil Moisture Content (SMC) was fixed to 15%, the soil height standard deviation σ_z to 1.5 cm, and its correlation length to 5 cm. On the other hand, we have verified that, at 45° incidence angle, changing their values in the ranges $10 \leqslant \mathrm{SMC} \leqslant 20\%$ and $0.5 \leqslant \sigma_z \leqslant 2$ cm, the theoretical backscattering coefficient changes only for biomasses lower than 60 t/ha and mainly at vertical polarization: effects are limited by less than 0.5 dB for Soil Moisture and by 1.5 dB for soil roughness variations.

Fig. 2 shows the simulated trends of σ^0 at the three linear polarizations and, reported for the sake of comparisons, also the polynomial regressions given by Imhoff (1995). In general, the increasing trend of σ^0 at the three polarizations is reproduced by the model and shows the saturation limit of the radar measurements which become almost insensitive to biomass beyond a certain limit. At

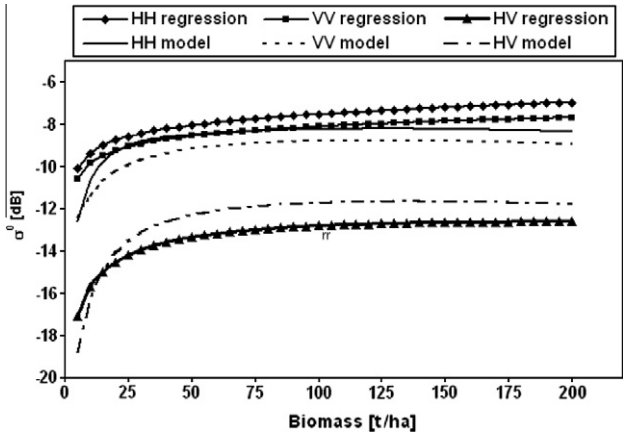

Fig. 2. Comparison between model results and regression curves of the AIRSAR L-band measurements over the broadleaf evergreen forests in Hawaii (Imhoff, 1995).

large values of biomass, the model overestimates the cross-polarized backscattering, while a slight underestimation is present in the co-polarized cases. The overall Root Mean Square (RMS) of the model error is 0.95 dB, indicating a generally good correspondence. The positive results of the backscattering test also allow us to be confident upon the assumptions made in Section 2.2 about the geometrical forest parameters of the Hawaii site.

3.3. Extension of simulations to the specular case

Up to now, no results of GNSS-R measurements over forests were published, so that it is not possible to assess the potentiality of this technique in biomass monitoring by means of experimental data. To reach this goal, the electromagnetic model developed at Tor Vergata is used. In the following, the specular bistatic coefficient of the same Hawaiian forest site is simulated and the relative contributions of the coherent and incoherent components in the specular direction are also highlighted.

We assumed that, if the observed area is flat (i.e., no topographic relief is present), contributions to specular reflection come mainly from the first Fresnel zone. The latter is traditionally defined as the locus of points, surrounding the specular reflection point, which reflect waves with phase shifts $\leqslant\pi$ with respect to the one reflected by the specular point itself. The waves reflected by different points on a surface interfere constructively if their paths differ by less than half a wavelength, otherwise they add with alternatively destructive and constructive interference. Since the destructive contributions of some points outside the first Fresnel zone are balanced by the constructive contributions of other points, it is usually assumed that the area responsible of reflection is only that of the first Fresnel zone (Beckmann and Spizzichino, 1963). In other words, a reflection that we think of as coming from a single point is actually being reflected from an ellipse with semiaxes a and b given by the following equation (when the transmitter height H_T is much larger than the receiver height H_R, and neglecting the earth curvature):

$$b = \frac{\sqrt{\lambda H_R \cos\vartheta_i}}{\cos\vartheta_i}, \quad a = \frac{b}{\cos\vartheta_i} \tag{4}$$

These formulas are usually quoted in GNSS-R studies (Masters et al., 2004; Katzberg et al., 2006) and can be derived as in Caparrini (1998) from the expression of the geometrical locus of points with constant delays, given at p. 287 of Beckmann and Spizzichino (1963). The flat earth approximation can be considered valid for low incidence (high elevation) angles (Hajj and Zuffada, 2003).

Besides the coherent component coming from specular reflection by the first Fresnel zone, a diffuse component can be also present in the GNSS-R signal. It comes from the so-called glistening area, which is defined as the area for which the scattered power has dropped down by a factor $1/e$ (−4.3 dB) with respect to the specularly reflected one (Beckmann and Spizzichino, 1963). In the case of ocean surfaces, the diffuse contribution is described as the one produced by tilted facets on the surface and properly oriented to redirect the electromagnetic wave towards the receiver. Indeed, a slope probability function is usually introduced to model this contribution (see the Kirchhoff approximation) which describes scattering caused by roughness of the surface at scales comparable or larger than the incoming wavelength. We remark that, under these conditions, the coherent component is largely overpassed by the incoherent one and coherent scattering is consequently neglected. The roughness scales typical of land surfaces are well below the GNSS wavelength so that, unless topographic effects are present, the diffuse component does not arise from properly oriented slopes, and incoherent scattering is theoretically described by the Small Perturbation Model and the Integral Equation Method. As a consequence, while ocean surfaces own a glistening area that may extend over several delays with respect to the specular one, land surfaces do not own a glistening area since, as it will be shown by the following simulations, diffuse scattering from bare and vegetated soils is usually much lower than the coherent component.

In Fig. 3 the linear co-polarized response in the specular direction is represented as a function of the standing forest biomass, for an incidence angle of 20°: the steep decreasing trend of the specular scattering coefficient is due to the strong soil reflection, which suffers from an increasing attenuation due to the increasing forest biomass. Note that, in Fig. 3, the total scattering coefficient, i.e., including both coherent and incoherent contributions, is superimposed on the curve that reproduces soil coherent scattering coefficient. This is a consequence of the fact that the latter keeps values larger than 10 dB, which are significantly higher than any incoherent contribution, i.e., coming from both vegetation volume and underlying ground. In particular, incoherent scattering from soil can be always considered negligible, while volume scattering may become a non-negligible contribution when vegetation biomass is large.

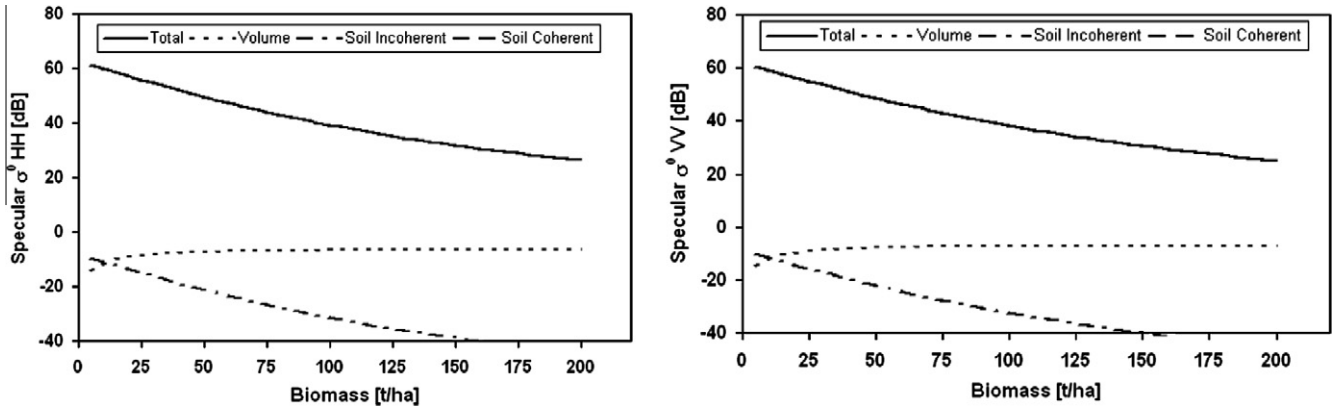

Fig. 3. Simulated specular scattering coefficient of the first Fresnel zone for the broadleaf evergreen forests in Hawaii. Incidence and observation angle $\vartheta_i = 20°$, HH (left) and VV (right) polarizations.

4. Bistatic system with a GNSS receiver

4.1. Single scattering approximation

In order to simulate the circularly polarized signal transmitted by a GNSS satellite, the Matrix Doubling procedure of the Tor Vergata model calls for an extension to a fully polarimetric version (Bracaglia et al., 1995) which requires scattering and extinction matrices with dimensions 4 times bigger than in the linear polarization version. The requested computational effort is therefore heavily increased and it is justified only if multiple scattering processes contribute significantly to the overall scattering. We have checked that this is not the case for the GNSS-R configuration, so that the Tor Vergata model can be applied in a simplified single scattering form, wheareas allowing introduction of circular polarizations.

Let us consider a linearly q-polarized field E_q^i that is impinging upon a dielectric scatterer from a direction identified with angles ϑ_i and ϕ_i. The particle scatters in the direction identified with angles ϑ_s and ϕ_s a p-polarized field E_p^s which behaves as a spherical wave and, at a distance R from the scatterer, is expressed by

$$E_p^s(\vartheta_s, \varphi_s) = \frac{e^{ikR}}{R} f_{pq}(\vartheta_i, \varphi_i; \vartheta_s, \varphi_s) E_q^i(\vartheta_i, \varphi_i) \tag{5}$$

f_{pq} is called the scattering amplitude and it is related to the bistatic scattering cross section σ_{pq} and the extinction cross section σ_{ep} of the scatterer by

$$\sigma_{pq}(\vartheta_i, \varphi_i; \vartheta_s, \varphi_s) = 4\pi |f_{pq}(\vartheta_i, \varphi_i; \vartheta_s, \varphi_s)|^2,$$
$$\sigma_{ep}(\vartheta_i, \varphi_i) = \frac{4\pi}{k} \Im\{f_{pp}(\vartheta_i, \varphi_i; \pi - \vartheta_i, \varphi_i)\} \tag{6}$$

where $\Im$ stands for the imaginary part operator and k is the wavenumber.

Let us now consider the forest crown as a collection of scatterers of different shapes, sizes, orientations and densities. Neglecting multiple scattering, we introduce the normalized crown bistatic scattering cross section and the normalized crown extinction cross section:

$$\sigma_{pq}^{crown}(\vartheta_i, \varphi_i; \vartheta_s, \varphi_s) = \sum_j N_j^{crown} \sigma_{jpq}(\vartheta_i, \varphi_i; \vartheta_s, \varphi_s),$$
$$\tau_p^{crown}(\vartheta_i, \varphi_i) = \sum_j N_j^{crown} \sigma_{ejp}^{crown}(\vartheta_i, \varphi_i) \tag{7}$$

Both parameters are normalized to the underlying area, and the second one is also referred to as optical depth. N_j^{crown} is the density per unit area of the j-th scatterer type in the crown layer, i.e., disks, needles or cylinders (N_j^{crown} is the conventional density per unit volume multiplied by the crown height), and

$$\sigma_{jpq}(\vartheta_i, \varphi_i; \vartheta_s, \varphi_s) = 4\pi \left\langle |f_{jpq}^{crown}(\vartheta_i, \varphi_i; \vartheta_s, \varphi_s)|^2 \right\rangle \tag{8}$$

$$\sigma_{ejp}^{crown}(\vartheta_i, \varphi_i) = \frac{4\pi}{k} \Im\left\{ \left\langle f_{jpp}^{crown}(\vartheta_i, \varphi_i; \pi - \vartheta_i, \varphi_i) \right\rangle \right\} \tag{9}$$

f_{jpq}^{crown} is the complex scattering amplitude of the j-th scatterer type in the crown. Brackets stand for dimension and orientation averaging.

The power density scattered at distance R by an illuminated area A of a forest crown with height h, is given by (Ulaby et al., 1982)

$$|E_p^s(\vartheta_s, \varphi_s)|^2 = \frac{A}{4\pi R^2} |E_q^i(\vartheta_i, \varphi_i)|^2 \int_0^h \sigma_{pq}^{crown}(\vartheta_i, \varphi_i; \vartheta_s, \varphi_s)/h \cdot e^{-\tau_q^{crown}(\vartheta_i)/(h\cos\vartheta_i)z} \cdot e^{-\tau_p^{crown}(\vartheta_s)/(h\cos\vartheta_s)z}\, dz \tag{10}$$

From integration of the above equation the bistatic crown volume scattering coefficient can be derived and, specifying for the specular direction, it is

$$\sigma_{pq}^{volume}(\vartheta_i, \varphi_i) = \frac{4\pi R^2 |E_p^s(\vartheta_i, \varphi_i)|^2}{A |E_q^i(\vartheta_i, \varphi_i)|^2} = \frac{\sigma_{pq}^{crown}(\vartheta_i, \varphi_i; \vartheta_i, \varphi_i) \cdot \cos\vartheta_i}{\tau_p^{crown}(\vartheta_i) + \tau_q^{crown}(\vartheta_i)} \times (1 - e^{-\tau_q^{crown}(\vartheta_i)/\cos\vartheta_i} e^{-\tau_p^{crown}(\vartheta_i)/\cos\vartheta_i}) \tag{11}$$

We now introduce a trunk layer below the crown which attenuates electromagnetic waves. Because of their large dimensions, trunks produce mainly forward scattering, and for this reason direct upward scattering from trunks can be neglected. Following the considerations drawn at

the end of the previous section, the specular scattering coefficient of the whole forest canopy can be formulated by the sum of two contributions:

$$\sigma_{pq}^{0sp}(\vartheta_i,\varphi_i) = \frac{1}{L_p^{trunk}(\vartheta_i)}\frac{1}{L_p^{crown}(\vartheta_i)}\sigma_{cohpq}^{soil}(\vartheta_i,\varphi_i;\vartheta_i,\varphi_i)\frac{1}{L_q^{trunk}(\vartheta_i)}\frac{1}{L_q^{crown}(\vartheta_i)} + \frac{\sigma_{pq}^{crown}(\vartheta_i,\varphi_i;\vartheta_i,\varphi_i)\cdot\cos\vartheta_i}{\tau_p^{crown}(\vartheta_i)+\tau_q^{crown}(\vartheta_i)}\left(1-\frac{1}{L_p^{crown}(\vartheta_i)}\frac{1}{L_q^{crown}(\vartheta_i)}\right) \tag{12}$$

The first term represents coherent scattering in the specular direction, the second term represents incoherent volume scattering. (From now on, the angular dependence will be understood, since the specular direction only is taken into account.)

In Eq. (12) σ_{coh}^{soil} is the soil coherent scattering coefficient (simulated accordingly to the theory developed in Fung and Eom, 1983) which is attenuated two times by the vegetation, made up of a crown and a trunk layer: $\frac{1}{L^{crown}}$ and $\frac{1}{L^{trunk}}$ are the one way loss factors of, respectively, the crown and the trunks. They are related to the normalized extinction cross section by means of $L^{layer} = e^{-\tau^{layer}/\cos\vartheta_i}$, where *layer* is *crown* or *trunk*.

τ^{trunk} is computed by averaging the extinction (σ_{ej}) cross sections of the single scatterers inside the trunk layer, over all dimensions, by means of the following relationships:

$$\tau_p^{trunk} = \sum_j N_{Tj}\sigma_{ejp}^{trunk} \tag{13}$$

$$\sigma_{ejp}^{trunk} = \frac{4\pi}{k}\Im\left\{\left\langle f_{jpp}^{trunk}(\vartheta_i,\varphi_i;\pi-\vartheta_i,\varphi_i)\right\rangle\right\} \tag{14}$$

f_{jpq}^{trunk} is the complex scattering amplitude of the j-th trunk at incident and scattering q and p polarizations. N_{Tj} is the density per unit area of trunks with the j-th *dbh*, within the distribution defined in Section 2.2. (For the Hawaii site $N_T = \sum_j N_{Tj}$ with N_T defined in Eq. (2).)

For circularly polarized incident and scattered fields, the scattering cross sections are obtained from a suitable linear combination of the scattering amplitudes $f_{VV}, f_{HH}, f_{HV}, f_{VH}$ (Ruck et al., 1970). The normalized circular extinction cross section τ_C is obtained according to the following procedure. If an elliptically polarized wave is propagating through a vegetation layer, the loss factor can be expressed as in Lopes et al. (1991):

$$\frac{1}{L_p^{layer}} = c_V^2\exp(-\tau_V^{layer}\sec\vartheta_i) + c_H^2\exp(-\tau_H^{layer}\sec\vartheta_i) + 2c_Vc_H\cos(\beta_H^{layer}-\beta_V^{layer}) \times \exp(-0.5(\tau_V^{layer}+\tau_H^{layer})\sec\vartheta_i) \tag{15}$$

where *layer* is *trunk* or *crown* and

$$\beta_p^{layer} = \frac{2\pi}{k}\sum_j N_j^{layer}\Re\left\{\left\langle f_{jpp}^{layer}(\vartheta_i,\varphi_i;\pi-\vartheta_i,\varphi_i)\right\rangle\right\} \tag{16}$$

with $p = H$ or V or circular, and $\Re$ being the real part operator. For a V polarized wave $c_V = 1$ and $c_H = 0$; for an H polarized wave $c_V = 0$ and $c_H = 1$; for a circularly polarized wave $c_V = 1/2$ and $c_H = 1/2$. Note that the loss factor is the same for a left circularly polarized wave and a right circularly polarized wave. Given an incident circularly polarized wave, the normalized circular extinction cross section τ_C can be derived by the inversion:

$$\tau_C^{layer} = \cos\vartheta_i\cdot\ln(L_C^{layer}) \tag{17}$$

In order to consider the wave depolarization, which can also occur during propagation through the vegetation layer, the depolarization factor D (Lopes et al., 1991) has been introduced:

$$D_p^{layer} = \left|\exp\left(-\frac{1}{2}\tau_V^{layer}\sec\vartheta_i\right) - \exp\left(-\frac{1}{2}\tau_H^{layer}\sec\vartheta_i\right)\right|^2 c_Vc_H \tag{18}$$

It is now possible to account for the wave impinging on the soil at, let us say, circular right polarization which is composed of the incident right polarized wave affected by vegetation attenuation (through the loss factor $1/L$), but also of the left polarized incident wave depolarized while propagating through vegetation. Similarly, the power scattered by soil suffers from attenuation and depolarization before reaching the receiver. As a consequence, for circularly polarized waves, the first term in Eq. (12) becomes (the subscripts R and L stand for Right and Left polarization):

$$\begin{aligned}\sigma_{RR}^{soil} &= \left(\frac{1}{(L_C^{crown})^2(L_C^{trunk})^2} + (D_C^{crown})^2(D_C^{trunk})^2\right)\sigma_{cohRR}^{soil} + 2\frac{D_C^{crown}}{L_C^{crown}}\frac{D_C^{trunk}}{L_C^{trunk}}\sigma_{cohRL}^{soil}\\ \sigma_{RL}^{soil} &= \left(\frac{1}{(L_C^{crown})^2(L_C^{trunk})^2} + (D_C^{crown})^2(D_C^{trunk})^2\right)\sigma_{cohRL}^{soil} + 2\frac{D_C^{crown}}{L_C^{crown}}\frac{D_C^{trunk}}{L_C^{trunk}}\sigma_{cohRR}^{soil}\end{aligned} \tag{19}$$

where it is assumed that $\sigma_{RL} = \sigma_{LR}$ and $\sigma_{LL} = \sigma_{RR}$, due to the azimuthal symmetry of the vegetation canopy.

First of all, this simplified single scattering model has been tested comparing the simulations performed at linear polarizations in the specular directions against the simulations performed applying the general Tor Vergata model, described in Section 2, based on the Matrix Doubling algorithm. The latter allows to include multiple scattering contributions within the crown and also multiple interactions between the soil and the crown itself. The difference between the results obtained by the two methods is very low with respect to the dynamic range: the maximum difference occurs at the largest biomass values and it is equal to 1.2 dB at VV polarization and to 0.5 dB at HH polarization. This result is obtained because the specular scattering is contributed mainly by the attenuated coherent scattering

from the soil and multiple scattering effects introduced by vegetation are negligible. On the other hand, we point out that the multiple scattering contributions could not have been neglected in the monostatic simulations, at least when the volume contribution is the most important one (Ferrazzoli and Guerriero, 1995).

4.2. Simulations of GNSS reflected power

As we mentioned earlier, the specular scattering coefficient due to the coherent scattering from the soil depends on the transmitter and receiver parameters (Fung and Eom, 1983), i.e., the antenna beamwidths and their heights. Indeed, applying the scattering coefficient definition to a coherent process means to transfer the antenna effects into a parameter which should represent the object scattering properties only. In order to use a physical quantity which is more useful from the application point of view, in the following simulations we will make reference to the power which reaches the receiving antenna. To this end, the classical bistatic radar equation is used to compute the power measured by the receiver antenna: an Equivalent Isotropic Radiated Power (EIRP) by the GNSS transmitter equal to 27 dBW is assumed to be incident over the observed surface (Bao-Yen Tsui, 2005). Coherent power comes from an area equal to the first Fresnel zone and characterized by the coherent specular bistatic scattering coefficient calculated by means of the model described previously. In particular, for transmitter and receiver heights fixed, respectively, to $H_T = 20{,}000$ km and $H_R = 600$ km, the region where coherent reflection takes place has an extension of about 0.35 km^2 at nadir.

In order to evaluate incoherent power we applied the bistatic radar equation to the equi-delay ellipse surrounding the specular point and corresponding to ½ chip delay of the C/A code. For the above receiver and transmitter height, this is an area of about 500 km^2 at nadir. We then supposed that the bistatic scattering coefficient of this area was isotropic and equal to the specular one: this represents an upper bound since bistatic scattering is usually at its maximum in the specular direction.

In the following simulations, a receiving antenna gain equal to 25 dB was supposed (this is an arbitrary value that, however, affects the power simulation in dBW only by a constant factor and does not change its sensitivity to biomass). Additional processing gains, such as coherent or incoherent integration, were understood: that is, the expected value of the received signal is considered, provided the proper noise and speckle mitigation approaches are carried out.

The simulations of the co- and cross-circularly polarized powers at an angle $\vartheta_s = \vartheta_i = 20°$ are reported in Fig. 4 as a function of biomass of the Hawaii deciduous forest. On the left of Fig. 4, simulations of the two components of the RL power are plotted. It can be observed that, unless vegetation is very dense, it is not possible to define a glistening area since the incoherent power (from both volume and soil) is well below −4.3 dB of the coherent power. Experimental data support this outcome: GNSS-R waveforms collected over land surfaces (Masters et al., 2004) did not show spreading to delays longer than the specular one, and measurements performed with the Interferometric Technique (Rodriguez-Alvarez et al., 2009) were based on the coherency of the specularly reflected signal.

From Fig. 4 we also observe that the coherent RR polarization power is about 30 dB lower than the RL one, since vertical and horizontal reflectivities have opposite phases whose combination tends to cancel coherent reflection by soil at RR polarization. As a consequence, the RR signal is prevalently dominated by incoherent scattering, quickly reaching a saturation values which is very low. Therefore, detection of RR polarization appear more critical, so that the following simulations will concern RL polarization only.

5. Sensitivity study

In this section, the sensitivity of a GNSS reflected signal to forest biomass will be studied for various incidence angles, soil parameters and *dbh* distributions. The effects of incidence angle are reported in Fig. 5 which shows that at the higher incidence angles the *RL* signal owns a large

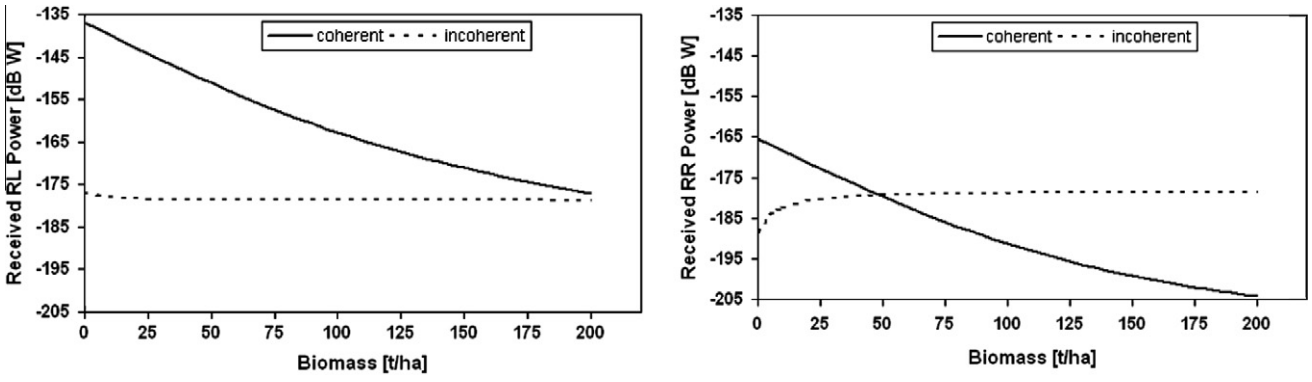

Fig. 4. Received power at circular polarizations vs. biomass. $\vartheta_i = 20°$, $\sigma_z = 1.5$ cm, SMC = 15%, receiving antenna gain $G = 25$ dB. (left) RL polarization; (right) RR polarization.

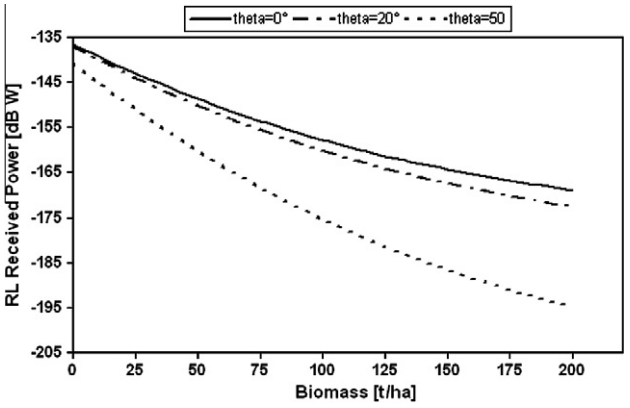

Fig. 5. Received power at RL polarization vs. the biomass of the Hawaii forest. The three curves correspond to three incidence angles ($\vartheta_i = 0°$, 20° and 50°). $\sigma_z = 1.5$ cm, SMC = 15%, receiver antenna gain $G = 25$ dB.

dynamic range, but it carries lower power which can result in a very low SNR. For this reason, low observation angles seem to be better suited to biomass monitoring, and we remark that for $\vartheta_i \sim 20°$, the sensitivity of σ^0_{RL}, although is lower than the one at higher angles, may reach an appreciable value of about 2 dB for an increase of 10 t/ha.

In order to appreciate the effects of soil parameters, Fig. 6 reports the simulated power at $\vartheta_i = 20°$ for two different values of Soil Moisture Content and two different values of the height standard deviation. This plot confirms that the received power is stronger for lower biomass value and it shows that power decreases with decreasing soil moisture or with increasing roughness. However, the effects of all soil variables are low with respect to the dynamic range related to variations of forest biomass.

All previous simulations of GNSS-R measurements were performed assuming the Hawaii forest as a case study, i.e., using the same forest parameters used in Section 3.2 to compare the model results with the monostatic measurements reported in Imhoff (1995). In order to simulate different environmental conditions, in Fig. 7 the effect of the forest *dbh* is studied. In particular, specular measurements were simulated concerning forests with a

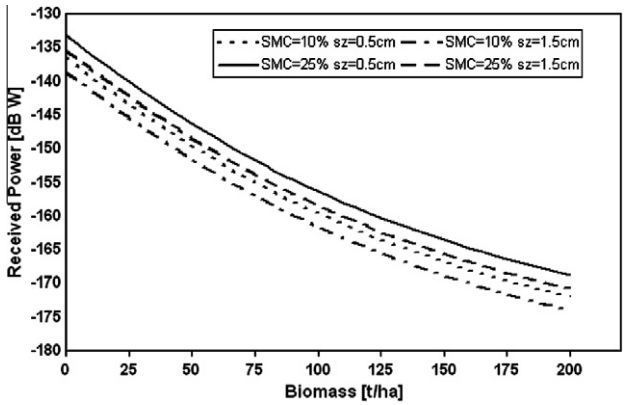

Fig. 6. Received power at $\vartheta_i = 20°$, RL polarization, vs. the biomass of the Hawaii forest. The curves correspond to different soil conditions as indicated in the legend.

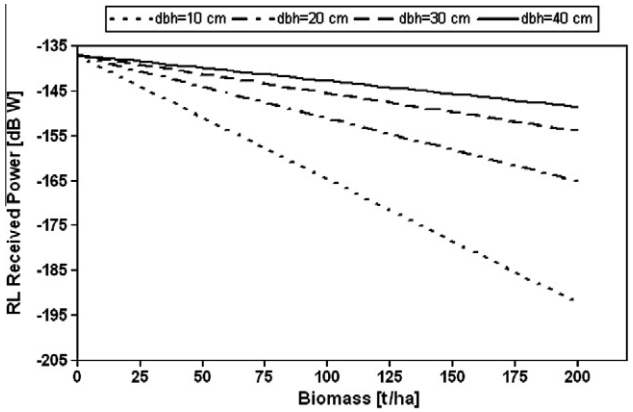

Fig. 7. Received power at RL polarization vs. the biomass of forest with four different dbh_{mean}: 10, 20, 30, 40 cm, *dbh* standard deviation $\sigma_{dbh} = 1$ cm. $\vartheta_i = 20°$, $\sigma_z = 1.5$ cm, SMC = 15%.

Gaussian *dbh* distribution but with different mean *dbh*. For the sake of simplicity, the trees were ideally supposed to be all of the same size, i.e., given a dbh_{mean} value, the standard deviation of *dbh* was taken to be equal to 1 cm, and the biomass variation is obtained increasing the tree density. The simulations show that the sensitivity of the GNSS-R signal is dependent on the contextual forest parameters, i.e., *dbh* and density. In particular, for a given biomass, lower signal powers are received when the trees are very small and very numerous. The presence of larger and fewer trees (larger dbh_{mean} values) reduces attenuation and consequently the sensitivity to biomass, upon which it is strictly dependent. Nevertheless, the dynamic range of the RL polarized reflected power at low incidence angle remains larger than 10 dB, even in the worst case.

6. Conclusions

In this paper, theoretical simulations of the specular scattering coefficient of forests were performed in order to evaluate the potential of the GNSS-R technique for biomass monitoring. A deciduous forest site in Hawaii, for which measurements were available in the literature, has been considered to test the monostatic simulations of the model and, then, to analyse the behaviour of the simulations in the specular direction. A simplified model able to take the GNSS circular polarization into account have been introduced and computations have shown that forests do not mask the *RL* coherent specular reflection from soil. This contribution turns out to be larger than incoherent scattering from the vegetation volume and the underlying soil, thus allowing to monitor forest biomass thanks to its attenuation effects. Depending on the observation angle and the forest density, the reflected power can be significantly high to be detected. In particular, specular measurements at low incidence angles and RL polarization are more suitable for forest applications, since they keep a significant sensitivity to biomass without reaching extremely low values of received power.

Acknowledgements

This work has been supported by ESA/ESTEC under contract 19173/05/NL/GLC. The authors wish to thank Dr. Nicolas Floury for his useful suggestions.

References

Bao-Yen Tsui, J. Fundamental of Global Positioning System Receivers. A Software Approach. Wiley, Hoboken, NJ, 2005.

Beckmann, P., Spizzichino, A. The Scattering of Electromagnetic Waves from Rough Surfaces. Artech House, Norwood, MA, 1963.

Bracaglia, M., Ferrazzoli, P., Guerriero, L. A fully polarimetric multiple scattering model for crops. Remote Sens. Environ. 54, 170–179, 1995.

Cannell, M.G.R. World Forest Biomass and Primary Production Data. Academic Press, New York, 1982.

Caparrini, M. Using reflected GNSS signals to estimate surface features over wide ocean areas. ESTEC Report no. 2003, 1998.

Chen, K.S., Wu, T.-D., Tsang, L., Li, Q., Shi, J., Fung, A.K. Emission of rough surfaces calculated by the Integral Equation Method with comparison to three-dimensional Moment Method simulations. IEEE Trans. Geosci. Remote Sens. 41, 90–101, 2003.

Della Vecchia, A., Ferrazzoli, P., Wigneron, J.-P., Grant, J.P. Modeling forest emissivity at L-band and a comparison with multifrequency measurements. IEEE Geosci. Remote Sens. Lett. 4, 508–512, 2007.

Della Vecchia, A., Ferrazzoli, P., Guerriero, L., Rahmoune, R., Paloscia, S., Pettinato, S., Santi, E. Modeling the multifrequency emission of broadleaf forests and their components. IEEE Trans. Geosci. Remote Sens. 42, 260–272, 2010.

Egido, A., Martin, C., Felip, D., Garcia, M., Caparrini, M., Farrés, E., Ruffini, G. The SAM sensor: an innovative GNSS-R system for soil moisture retrieval, in: Proceedings of NAVITEC08, Noordwijk, NL, 2008.

Eom, H.J., Fung, A.K. A scatter model for vegetation up to Ku-band. Remote Sens. Environ. 15, 185–200, 1984.

Eom, H.J., Fung, A.K. Scattering from a random layer embedded with dielectric needles. Remote Sens. Environ. 19, 139–149, 1986.

Ferrazzoli, P., Guerriero, L. Radar sensitivity to tree geometry and woody volume: a model analysis. IEEE Trans. Geosci. Remote Sens. 33, 360–371, 1995.

Ferrazzoli, P., Guerriero, L. Passive microwave remote sensing of forests: a model investigation. IEEE Trans. Geosci. Remote Sens. 34, 433–443, 1996.

Ferrazzoli, P., Guerriero, L., Solimini, D. Simulating bistatic scatter from surfaces covered with vegetation. J. Electromagnet. Waves Appl. 14, 233–248, 2000.

Fung, A.K., Eom, H.J. Coherent scattering of a spherical wave from an irregular surface. IEEE Trans. Antennas Propagat. AP-31, 68–72, 1983.

Fung, A.K. Microwave Scattering and Emission Models and their Applications. Artech House, Norwood, MA, 1994.

Gleason, S., Hodgart, S., Sun, Y., Gommenginger, C., Mackin, S., Adjrad, M., Unwin, M. Detection and processing of bistatically reflected GPS signals from Low Earth Orbit for the purpose of ocean remote sensing. IEEE Trans. Geosci. Remote Sens. 43, 1229–1241, 2005.

Gleason, S. Detecting bistatically reflected GPS signals from Low Earth Orbit over land surfaces, in: Proceedings of IGARSS06, Denver, CO, 2006.

Hajj, G., Zuffada, C. Theoretical description of a bistatic system for ocean altimetry using the GPS signal. Radio Sci. 38, 1–19, 2003.

Imhoff, M.L. Radar backscattering and biomass saturation: ramifications for global biomass inventory. IEEE Trans. Geosci. Remote Sens. 33, 511–518, 1995.

Jenkins, J.C., Chojnacky, D.C., Heath, L.S., Birdsey, R.A. National-scale biomass estimators for United States tree species. Forest Sci. 49, 12–26, 2003.

Jin, S., Komjathy, A. GNSS reflectometry and remote sensing: new objectives and results. Adv. Space Res. 46 (2), 111–117, doi:10.1016/j.asr.2010.01.014, 2010.

Karam, M.A., Fung, A.K. Electromagnetic scattering from a layer of finite length, randomly oriented, dielectric, circular cylinders over a rough interface with application to vegetation. Int. J. Remote Sens. 9, 1109–1134, 1988.

Kasischke, E.S., Christensen, N.L., Haney, E.M. Modeling of geometric properties of loblobby pine tree stand characteristics for use in radar backscatter studies. IEEE Trans. Geosci. Remote Sens. 32, 800–822, 1994.

Katzberg, S.J., Torres, O., Grant, M.S., Masters, D. Utilizing calibrated GPS reflected signals to estimate soil reflectivity and dielectric constant: results from SMEX02. Remote Sens. Environ. 100, 17–28, 2006.

LeToan, T., Beaudoin, A., Riom, J., Guyon, D. Relating forest biomass to SAR data. IEEE Trans. Geosci. Remote Sens. 30, 403–411, 1992.

Le Vine, D.M., Meneghini, R., Lang, R.H., Seker, S.S. Scattering from arbitrarily oriented dielectric disks in the physical optics regime. J. Opt. Soc. Am. 73, 1255–1262, 1983.

Liang, P., Pierce, L., Moghaddam, M. Radiative transfer model for microwave bistatic scattering from forest canopies. IEEE Trans. Geosci. Remote Sens. 43, 2470–2483, 2005.

Lopes, A., Mougin, E., LeToan, T., Karam, M.A., Fung, A.K. A simulation study on the influence of leaf orientation on elliptically polarized microwave propagation in a coniferous forest. J. Electromagnet. Waves Appl. 5, 753–776, 1991.

Macelloni, G., Nesti, G., Pampaloni, P., Sigismondi, S., Tarchi, D., Lolli, S. Experimental validation of surface scattering and emission models. IEEE Trans. Geosci. Remote Sens. 38, 459–469, 2000.

Martin-Neira, M., Caparrini, M., Font-Rossello, J., Lannelongue, S., Serra Vallmitjana, C. The PARIS concept: an experimental demonstration of sea surface altimetry using GPS reflected signals. IEEE Trans. Geosci. Remote Sens. 39, 142–150, 2001.

Masters, D., Axelrad, P., Katzberg, S. Initial results of land-reflected GPS bistatic radar measurements in SMEX02. Remote Sens. Environ. 92, 507–520, 2004.

Peake, W. Interaction of electromagnetic waves with some natural surfaces. IRE Trans. Antennas Propag. AP-7, 324–329, 1959.

Pierdicca, N., Pulvirenti, L., Ticconi, F., Brogioni, M. Radar bistatic configurations for soil moisture retrieval: a simulation study. IEEE Trans. Geosci. Remote Sens. 46, 3252–3264, 2008.

Rodriguez-Alvarez, N., Bosch-Lluis, X., Camps, A., Vall-Ilossera, M., Valencia, E., Marchan-Hernandez, J.F., Ramos-Perez, I. Soil moisture retrieval using GNSS-R techniques: experimental results over a bare soil field. IEEE Trans. Geosci. Remote Sens. 47, 3616–3624, 2009.

Ruck, G.T., Barrick, D.E., Stuart, W.D., Krichbaum, C.K.. Radar Cross Section Handbook, vol. 1. Plenum Press, New York, 1970.

Ruffini, G. A brief introduction to remote sensing using GNSS reflections. IEEE Geosci. Remote Sens. Soc. Newslett., 15–21, March, 2006.

Ulaby, F.T., Moore, R.K., Fung, A.K. Microwave Remote Sensing, vol. II. Addison-Wesley, Reading, MA, 1982.

Zavorotny, V.U., Voronovich, A.G. Scattering of GPS signals from the ocean with wind remote sensing application. IEEE Trans. Geosci. Remote Sens. 38, 951–964, 2000a.

Zavorotny, V.U., Voronovich, A.G. Bistatic GPS signal reflections at various polarizations from rough land surface with moisture content, in: Proceedings of IGARSS00, Honolulu, HI, pp. 2852–2854, 2000b.

Zavorotny V., Masters D., Gasiewski A., Bartram B., Katzberg S., Axelrad P., Zamora, R. Seasonal polarimetric measurements of soil moisture using tower-based GPS bistatic radar, in: Proceedings of IGARSS03, Toulouse, F, pp. 781–783, 2003.